Available online at www.sciencedirect.com
ScienceDirect
Journal of the European Ceramic Society 31 (2011) 1131–1139
www.elsevier.com/locate/jeurceramsoc

Original Article

Effect of microstructure on the mechanical properties of liquid-phase-sintered silicon carbide at pre-creep temperatures

Estíbaliz Sánchez-González, Pedro Miranda *, Fernando Guiberteau, Antonia Pajares

Departamento de Ingeniería Mecánica, Energética y de los Materiales, Escuela de Ingenierías Industriales, Universidad de Extremadura, 06071 Badajoz, Spain

Received 4 August 2010; received in revised form 20 December 2010; accepted 10 January 2011
Available online 1 February 2011

Abstract

The effect of the microstructure on the mechanical properties of pressureless, liquid-phase-sintered (LPS) α-SiC ceramics above room-temperature was studied. LPS-SiC ceramics were fabricated with different microstructural features (grain size and morphology, and content of the intergranular phase), and their mechanical behaviour under contact stresses was evaluated by high temperature Hertzian testing (HTHT) from room temperature up to the creep temperature (1000 °C). The amount of intergranular phase was found to control the elasto-plastic properties of LPS-SiC at intermediate temperatures. Grain size and morphology had a significant influence only on toughness, since the crack bridging mechanism was enhanced by elongated grains, the more so the larger their size. Implications of these results for the design and fabrication of LPS-SiC ceramics with tailored contact-mechanical properties are discussed.

Keywords: Hertzian test; Silicon carbide; Mechanical properties; Contact fracture; Temperature dependence

1. Introduction

During the last decade, non-oxide ceramics such as silicon nitride and silicon carbide (SiC) have achieved a prominent position among structural ceramics for their exceptional properties. The attractive properties of SiC include great hardness and strength with moderate toughness,[1,2] high resistance to aggressive chemical attack, to oxidation[3,4] and to wear,[5,6] high thermal conductivity and thermal-shock resistance,[7] and excellent strength retention at high temperatures.[4,8–10] Thanks to these exceptional properties, SiC-based materials have found industrial application in muffle furnace linings, kiln parts, high-temperature heat exchangers,[11,12] etc.

Among the different fabrication routes, pressureless, liquid-phase-sintering (LPS) using oxide additives (Al_2O_3, Y_2O_3) is the most attractive, as being a straightforward and economical alternative—thanks to the reduced sintering times and temperatures (1750–2000 °C), and the avoidance of having to use pressure—which is able to preserve most of the remarkable mechanical and thermal properties of SiC ceramics. Although there have been various studies devoted to analyzing the mechanical behaviour of LPS-SiC ceramics, they have been limited to either ambient[1,13–19] or high/creep temperatures.[4,8,9,20,21] Thus, despite the usual working temperatures of SiC being in the intervening temperature range, this interval has been somewhat neglected in previous studies, with the exception of certain measurements of the dynamic elastic modulus.[22] The present work seeks to redress this deficiency by elucidating the role of microstructural variables such as grain size, grain aspect ratio, and content of the intergranular phase on the mechanical properties of LPS-SiC in this intermediate temperature range.

High-temperature Hertzian testing[23] (HTHT) was the experimental method selected for this task. This technique, based on Hertzian indentation in combination with finite element modelling (FEM), has been successfully applied to study the effect of temperature on the mechanical properties—such as Young's modulus, quasi-plastic yield stress, strain-hardening parameter, critical load for contact damage initiation, etc.—of zirconia (Y–PSZ),[24] alumina,[25] silicon nitride,[26] and zirconium diboride.[27] Here, the HTHT technique was applied to study the evolution with temperature from 25 °C to 900 °C of the mechanical properties of 4 LPS-SiC materials with different microstructures. The results of the study clarify the relationship between microstructure and mechanical properties in LPS-SiC

* Corresponding author.
E-mail address: pmiranda@unex.es (P. Miranda).

0955-2219/$ – see front matter © 2011 Elsevier Ltd. All rights reserved.
doi:10.1016/j.jeurceramsoc.2011.01.003

in this temperature range, and to provide guidelines for the design of SiC materials with tailored mechanical properties for applications above room temperature.

2. Materials and experimental method

2.1. Material processing

Four different types of LPS-SiC materials were fabricated for this study. As reference material, one LPS-SiC was fabricated from commercial submicrometre α-SiC powders (UF-15, H.C. Stark, Germany) and a 20 wt% of sintering additives (Al_2O_3:Y_2O_3) in the molar ratio (3:5) necessary to form yttrium aluminium garnet (YAG, $Y_3Al_5O_{12}$). This amount of additives ensures full densification upon sintering and facilitates microstructural evolution.[28] The powders were homogenized in ethanol on a roller-mixer for 24 h. The excess ethanol was then evaporated on a hot plate with constant stirring, and the resulting powders were further dried in a drying oven at 100 °C for 24 h. Green samples were prepared from the mixed powders by cold uniaxial pressing at 50 MPa followed by cold isostatic pressing at 350 MPa. Compacts were then placed in closed graphite crucibles containing coarse Al_2O_3 and SiC powders (used as powder beds to prevent mass loss during sintering), and then pressureless sintered in a graphite furnace. The sintering conditions were: a peak temperature of 1950 °C; heating and cooling rates of 10 and 20 °C/min, respectively; a hold time at peak temperature of 2 h; and a flowing argon atmosphere. The sintered materials were ground down by 1 mm to remove the adhered powder bed layer, and then rinsed clean with acetone and ethanol. Finally, the test surfaces of the resulting flat specimens were polished to 1 μm finish.

Three additional types of materials were prepared following a similar procedure but modifying one of the following processing parameters: additive content (5 wt% instead of 20 wt%), sintering time (5 h instead of 2 h), and starting powder size (using F-1200 SiC powders, from Navarro SiC S.A., Spain, with sizes greater than 15 μm instead of the submicrometre UF-15 from H.C. Stark). The samples will be labeled indicating these variables: starting SiC powder size (fine, fSiC, or coarse, cSiC), followed by the intergranular phase weight fraction (%), and the sintering time. Thus, for example, the reference material will be designated as fSiC-20-2 h.

2.2. Microstructural characterization

The microstructure morphology of the fabricated LPS-SiC ceramics was analyzed using conventional scanning electron microscopy (SEM S-3600N, Hitachi Ltd., Japan) on polished surfaces. Samples were plasma etched (K1050X, Emitech Ltd., UK) prior to metalization and observation, using a mixture of CF_4 + 4% O_2 for 3.5 h, to reveal the grain boundaries. Average grain size and aspect ratios were quantitatively evaluated by image analysis.

The phase composition of the materials was determined by Rietveld analysis from X-ray diffraction data (PW-1800, Philips, Holland) obtained using CuKα radiation (40 kV, 35 mA), following the procedure described by Ortiz et al.[29] The relative density of the fabricated materials was evaluated by Archimedes' method, taking into account the theoretical densities of SiC (3.213 g/cm^3), $Y_3Al_5O_{12}$ (4.544 g/cm^3), and $YAlO_3$ (5.370 g/cm^3).

2.3. Mechanical testing

Fabricated LPS-SiC materials were preliminarily characterized by Vickers-indentation tests to evaluate their hardness, H, and toughness, K_{IC}, at room temperature. All Vickers-indentation tests were performed in air using a hardness tester (MV-1, Matsuzawa, Tokyo, Japan) equipped with a Vickers diamond pyramid, with a maximum load (P) of 98 N and dwell time of 20 s. Five separate indentations were performed for each material. The length of the diagonals of the residual impression and the total length of the surface traces of the radial cracks were then measured under optical microscopy (Epiphot 300, Nikon, Tokyo, Japan). The hardness and the toughness were determined using standard formulae.[30]

HTHT tests[23] were performed on a universal testing machine (AG-IS 100 kN, Shimadzu Corp., Kyoto, Japan) with an attached vertical split furnace. A 3 mm radius hemispherical silicon nitride indenter and the flat specimen to be tested were respectively bonded to the upper and lower alumina push rods using alumina paste (Ceramabond 569, Aremco Products Inc., NY, U.S.A.). External push rod holders were cooled with circulating water and a refrigerated convection shield was attached to the top holder to protect the load cell. Multiple tests (more than 25) can be made on each specimen at any selected temperature thanks to the X-Y table onto which the bottom push rod holder is placed. In order to produce a clear residual impression of the contact area at peak load even under elastic conditions, the specimen surface was sputter-coated (Polaron SC7640, East Sussex, U.K.) before the tests with a thin metallic film of Au, Rh–Pd, or Pt, depending on the testing temperature.[23]

The system was heated, in an air atmosphere, at a rate of 6 °C/min, and held for 1 h at the testing temperature before indentation sequences at increasing peak loads (25 N to 10 kN) were performed, using a constant crosshead speed of 0.05 mm/min and no hold time. Test temperatures were selected below the point at which the effects of creep on the size of the residual impressions were noticeable. For this purpose, two 1000 N indentations were generated at each testing temperature, using two different crosshead speeds (0.05 mm/min and 0.005 mm/min). At 1000 °C the contact radius of the imprint at 0.005 mm/min was more than 10 μm larger than that at 0.05 mm/min, and thus all the data from this temperature were discarded. As a result, the test temperatures selected for this study were 25 °C, 400 °C, 800 °C and 900 °C.

Plots of indentation stress ($p_0 = P/\pi a^2$) versus indentation strain (a/r) for each temperature were obtained from optical measurements of the contact radius, a, from the corresponding residual impressions after cooling, for each peak load, P, and indenter radius, r. Note that these indentation stress–strain curves are independent of the indenter radius.[31,32] Young's mod-

ulus, E, at each prescribed temperature was determined from the linear region of the indentation stress–strain curve using the Hertzian relation for elastic contacts[32,33]:

$$p_0 = \frac{4E^*}{3\pi}\frac{a}{r}, \quad p_0 < 1.1Y \tag{1}$$

where Y is the yield stress and

$$\frac{1}{E^*} = \frac{1-\nu^2}{E} + \frac{1-\nu'^2}{E'} \tag{2}$$

with ν being the Poisson ratio, and where the primes indicate indenter properties at the test temperature, obtained in a previous work.[26] The Poisson ratio of LPS-SiC is taken to be 0.21, as estimated from Ref. 18.

Optical microscopy with Nomarsky contrast was used to examine *post-mortem* the surface contact damage—permanent quasi-plastic deformation, and cone and/or radial cracks.[32] The critical loads for crack initiation were determined as the lowest applied load at which cracking was observed. The difference between this load and that immediately lower was used as an estimate of the measurement uncertainty for the critical load estimation.

Critical loads for quasi-plastic damage initiation, P_Y, and their corresponding uncertainties, were calculated from the expression[32,33]

$$P_Y = \frac{9(1.1\pi Y)^3}{16E^{*2}}r^2 \tag{3}$$

where Y is the material's yield stress, whose values can be calculated by FEM as described below.

2.4. Finite element modelling

ABAQUS/Standard (SIMULIA, Providence, RI) FEM software was used to estimate the yield parameters of LPS-SiC at each temperature. The algorithm models a deformable silicon nitride half-sphere of 3 mm radius in axisymmetric contact with a flat SiC specimen of 15 mm thickness and 15 mm radius. The load applied to the half-sphere is increased incrementally up to a maximum of 10 kN. The specimen and sphere grids consist of a total of more than 20 000 linear axisymmetric quadrilateral elements with reduced integration. Element dimensions range from a minimum of 1 μm × 1 μm around the contact region to hundreds of microns in regions far from the contact. The following constitutive uniaxial elasto-plastic model[23] is assumed in the calculations:

$$\begin{aligned} \sigma &= E\varepsilon \qquad (\sigma < Y) \\ \sigma &= [(E/Y)^n Y]\varepsilon^n \quad (\sigma < Y) \end{aligned} \tag{4}$$

where n is the dimensionless strain-hardening coefficient, with value between 0 (fully plastic) and 1 (fully elastic). For each temperature the values of Y and n are iteratively adjusted by trial and error to fit the FEM calculated indentation stress–strain curve to the experimental data, using the values of E—determined as described in the previous section—and ν as input parameters.

2.5. Results and discussion

Fig. 1 shows SEM micrographs of polished surfaces of the four materials studied. The SiC grains and the intergranular phase are clearly delineated by plasma etching in these micrographs. All the materials appear to be almost fully dense, which is consistent with the measured densities (Table 1). The microstructure of the reference sample fSiC-20-2 h (Fig. 1a) consist of a majority of elongated grains (actually platelets) with some equiaxed grains (average aspect ratio 2.6, see Table 1). The reduced wt% of the intergranular phase in the fSiC-5-2 h sample is evident in the SEM micrograph of Fig. 1b. The reduced amount of liquid phase hampers the development of elongated grains during sintering (through SiC β → α transformation[28]) in this sample, and thus a distribution of mostly equiaxed grains is observed (average aspect ratio 1.8). The microstructure of the fSiC-20-5 h sample (Fig. 1c) shows that increasing the sintering time produces a noticeable grain growth (roughly increasing the average grain size by 50%, see Table 1) but does not otherwise modify the microstructural morphology (cf. Fig. 1a), which remains dominated by elongated grains (average aspect ratio is again 2.6). Finally, the sample fabricated from coarser powders, cSiC-20-2 h, exhibits an obviously coarse microstructure, but composed of purely equiaxed grains (Fig. 1d, average aspect ratio 1.5) because of the absence of 6H → 4H transformation in this material (see Table 1). This is probably due both to the large initial size and to a reduced amount of stacking faults in the starting powders, since it is the presence of such faults which promotes the transformation and subsequent change in the grain aspect ratio.[28,34]

Table 1 summarizes the nomenclature, relative density, grain size and morphology, composition of the intergranular phase, and SiC polytype composition for each of these four materials, as determined from the microstructural characterization performed (i.e., SEM, XRD, etc.). All the materials consisted solely of α-SiC (with different polytype compositions) with either YAG or yttrium aluminate (YAP, $YAlO_3$) as intergranular phase (small amounts of unreacted alumina are detectable in some cases).

To finish with the preliminary characterization of the LPS-SiC materials that were fabricated, Fig. 2 shows the results of the room-temperature Vickers tests. The hardness values are roughly the same (∼15 GPa) for all the materials with 20 wt% of intergranular phase, but there is a 60% increase (to ∼24 GPa) for the sample with less additives. This expected result is a consequence of the significantly greater hardness of the SiC grains (∼25 GPa[13]) relative to the intergranular phase (∼15 GPa[13,35,36]), whether it be YAG[35] or YAP.[36] Nonetheless, the hardness values of the LPS-SiC materials do not fit the rule-of-mixture model, and the hardness of materials containing 20 wt% intergranular phase appears to be governed by this softer, continuous phase. The indentation–toughness values show that the elongated-grain microstructures (fSiC-20-2 h and fSiC-20-5 h) are consistently tougher (by more than 50%) than the equiaxed (fSiC-5-2 h and cSiC-20-2 h) microstructures which were found to have the same toughness (1.4 ± 0.1 MPa m$^{1/2}$). This is because elongated grains produce more efficient crack-

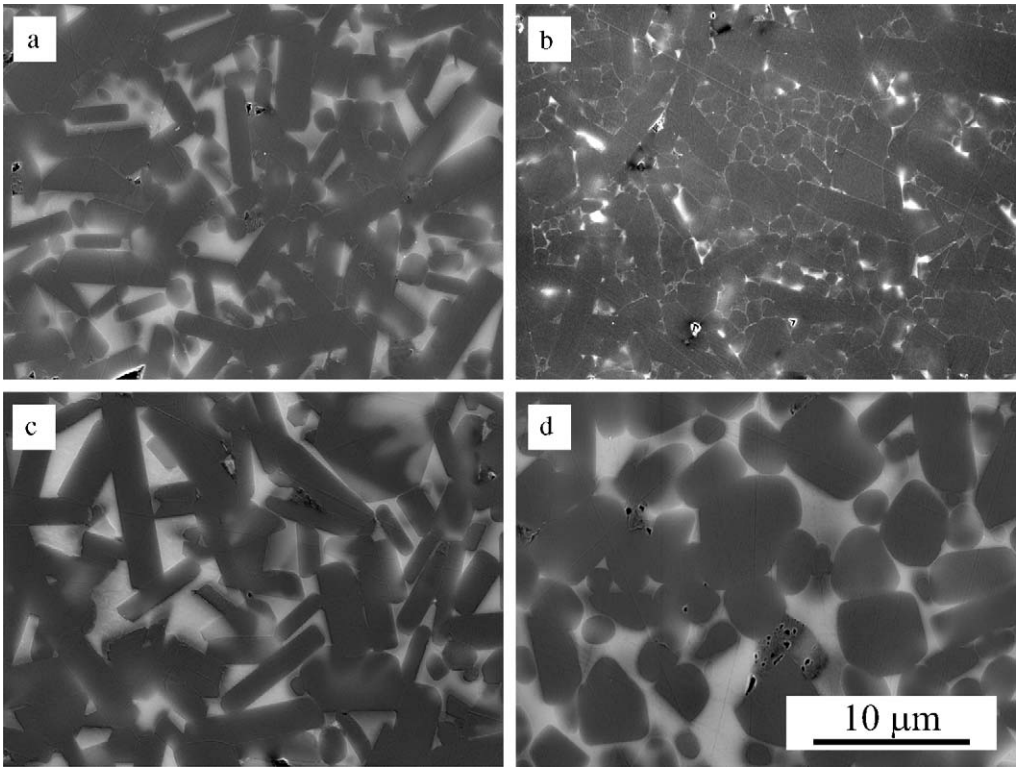

Fig. 1. SEM micrographs of polished surfaces of the four LPS-SiC materials studied: (a) fSiC-20-2 h, (b) fSiC-5-2 h, (c) fSiC-20-5 h and (d) cSiC-20-2 h. The SiC grains (dark grey) and the intergranular phase are clearly delineated by plasma etching.

Table 1
Microstructural features of the fabricated SiC materials.

Sample label[a]	ρ (%)	Grain size (μm)	Aspect ratio	Intergranular phase composition (wt%)	SiC polytypes (wt%)
fSiC-20-2 h	96	2.6	2.5	Alumina (1.2 ± 0.1) YAG (17.1 ± 0.3)	4H (37.0 ± 1.1) 6H (41.4 ± 1.0) 15R (3.3 ± 0.5)
fSiC-5-2 h	98	1.9	1.8	Alumina (0.8 ± 0.1) YAP (3.9 ± 0.1)	4H (26.5 ± 0.8) 6H (66.1 ± 1.3) 15R (2.7 ± 0.4)
fSiC-20-5 h	95	3.2	2.6	YAG (16.8 ± 0.7)	4H (54.3 ± 1.1) 6H (26.8 ± 0.7) 15R (2.1 ± 0.3)
cSiC-20-2 h	96	3.7	1.52	Alumina (1.0 ± 0.1) YAG (17.3 ± 0.5)	6H (79.9 ± 0.9) 15R (1.8 ± 0.1)

[a] Label indicates starting SiC powder size (fine, fSiC, or coarse, cSiC), followed by the intergranular phase weight fraction (%) and the sintering time.

bridging toughening,[37] the more so the larger the grain size, which explains why the fSiC-20-5 h sample seems to be slightly tougher than fSiC-20-2 h.

Indentation stress–strain curves for all the LPS-SiC materials are shown in Fig. 3 for the four test temperatures analyzed. Each point in these curves represents a single indentation performed at a prescribed peak load and temperature. The solid lines through the experimental data are FEM best-fits obtained as described in the preceding section. For each temperature, the initial part of the corresponding curve is linear but, at a certain indentation stress ($p_y \approx 1.1Y$), the data depart from linearity indicating the onset of quasi-plastic yield. A progressive decrease in both the slope of the linear part and the yield stress with temperature is apparent for all materials.

The Young's moduli calculated from the best-fit slopes to the linear regions of the stress–strain curves using Eq. (1) are plotted versus temperature in Fig. 4 for each LPS-SiC material. Calculated error bars are included, but they are sometimes smaller than the symbol size. The solid lines are included only as a guide to the eye. A slow linear decrease of the elastic modulus with increasing temperature is initially observed for all materials, but a sharper decay is observed above 800 °C. This modulus degradation above a certain temperature threshold is attributable to the activation of reversible grain boundary sliding and has been observed in other materials.[24–26] Also clear in Fig. 4 is the fact that the fSiC-5-2 h material exhibits an elastic modulus significantly greater (by 25%)—at room temperature its value is close to that of pure SiC (~440 GPa[12])—than the LPS-SiCs with a

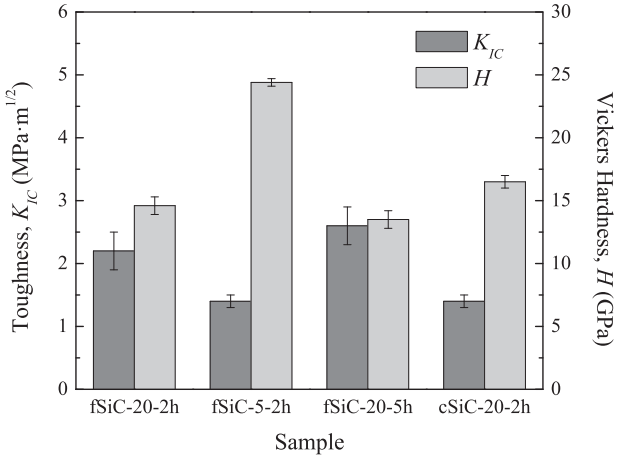

Fig. 2. Vickers tests measurements of the room-temperature hardness and toughness of the four LPS-SiC materials. The plot is of mean values with standard deviations as error bars.

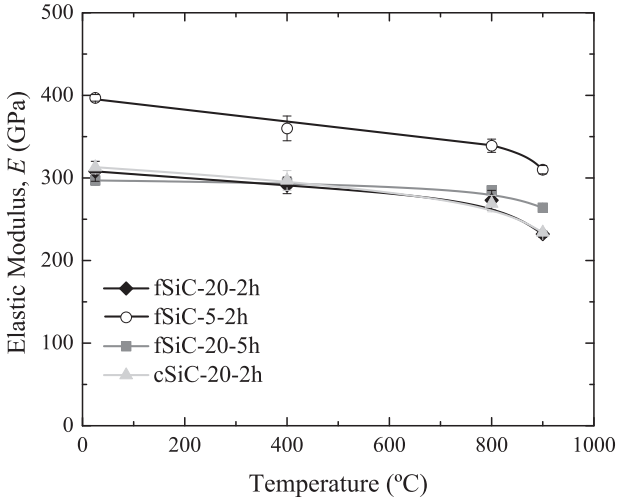

Fig. 4. Plot of Young's modulus versus temperature for all the LPS-SiC materials, as indicated. Calculated error bars are included, but are sometimes smaller than the symbol size. The solid lines are included only as a guide to the eye.

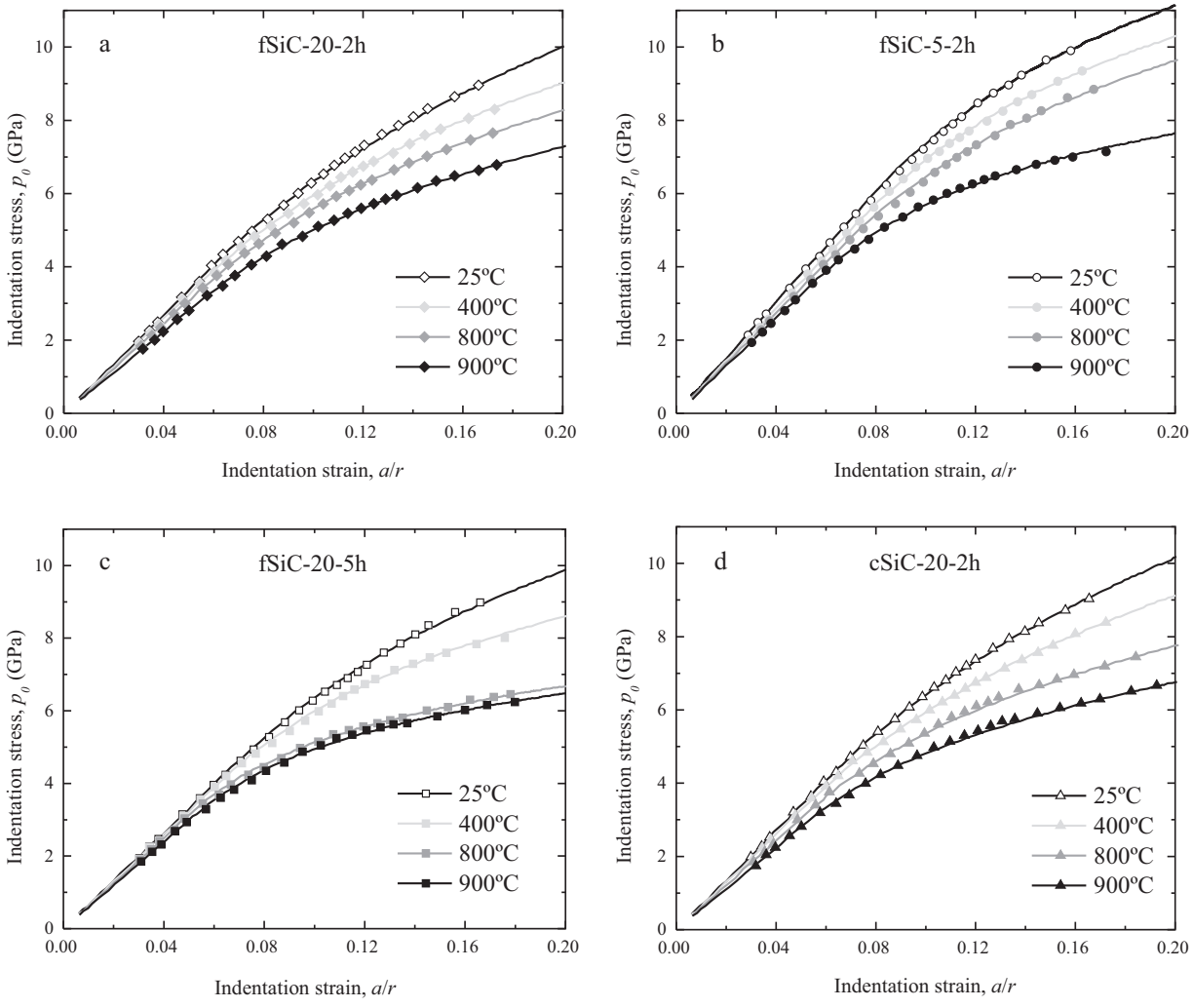

Fig. 3. Indentation stress–strain data at designated temperatures for all the LPS-SiC materials: (a) fSiC-20-2 h, (b) fSiC-5-2 h, (c) fSiC-20-5 h and (d) cSiC-20-2 h. Solid curves through experimental data are FEM best fits.

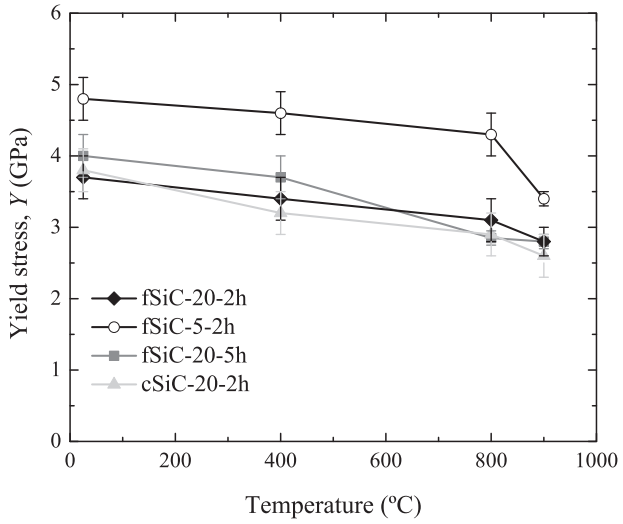

Fig. 5. Plot of FEM-estimated yield stress versus temperature for all the LPS-SiC materials. The error bars indicate the estimated maximum uncertainties and the solid lines connecting the data are included only as a guide to the eye.

greater intergranular phase content. The latter exhibit over the whole temperature range roughly similar values, which at room temperature are close to that of their YAG intergranular phase (∼282 GPa[35]).

Similar trends are observed for the yield stress values, determined from FEM as described in the previous section. These are shown in Fig. 5 as a function of temperature. The error bars indicate the estimated maximum uncertainties and the solid lines connecting the data are included only as a guide to the eye. As in the case of the Young's modulus, the yield stress decreases monotonically with increasing temperature. Also, the intergranular phase content plays a dominant role in determining its values, which are ∼25% higher for the fSiC-5-2 h sample, but with negligible differences between the other materials. The reason for this is that quasi-plasticity in these materials is attributed to microcracking and shear-faulting on the weak αSiC/YAG or αSiC/YAP interfaces due to the thermal residual stresses, and these are known to increase with the volume fraction of intergranular phase.[38] Finally, a significant drop or accelerated degradation of the yield stress is appreciable in the fSiC-5-2 h sample above 800 °C, although this is not so evident for the rest of the materials. This could be attributable to the degradation of grain boundary strength that ultimately leads to the onset of creep at around 1000 °C. It is worth noting that while creep is usually difficult to detect below 1300 °C for LPS-SiC,[8] here it is already noticeable at 1000 °C due to the higher pressures involved in Hertzian testing (above 1 GPa) compared to conventional creep tests (usually well below 500 MPa[8,20,21]).

The strain-hardening parameter values obtained from FEM were low ($n \leq 0.3$) in all materials at all temperatures. Further than that, given the large uncertainties (±0.1), no clear correlation between the values of this parameter and the microstructural features of the tested materials could be established.

Apart from allowing one to evaluate elasto-plastic properties of the tested materials such as those already discussed, with the HTHT technique one can investigate the evolution of

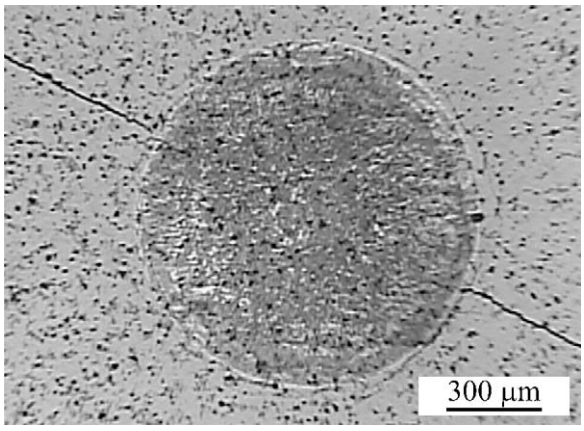

Fig. 6. Optical micrograph showing surface Hertzian damage induced on the fSiC-20-2 h material with a 3 mm indenter radius and 7 kN load at 400 °C. All the forms of contact damage observed in the LPS-SiC materials are apparent: quasi-plastic deformation, ring cracks, and radial cracks.

contact damage. Fig. 6 shows an optical micrograph of the surface damage induced on the fSiC-20-2 h material with a 3 mm indenter radius and 7 kN load at 400 °C. All the forms of contact damage observed in the LPS-SiC materials are apparent in this micrograph: quasi-plastic deformations, evidenced by Nomarsky illumination (although not clearly noticeable in the figure) as a slight depression in the test surface, ring cracks surrounding the impression zone, and radial cracks.

Fig. 7 shows the critical loads for the initiation of quasi-plastic damage, P_Y, calculated from Eq. (3), as a function of temperature. The error bars in this plot were determined from the estimated uncertainties in Y and E, see Eq. (3), and the solid lines are included only as a guide to the eye. Since P_Y depends more strongly on Y, its behaviour closely resembles that of the yield stress (Fig. 5), exhibiting a strong decline with temperature due to the increase in the thermal energy available for the initiation of this type of damage. One again clearly observes the dominant role played by the amount of intergranular phase on the onset of quasi-plastic deformation in the LPS-SiC materials: the fSiC-

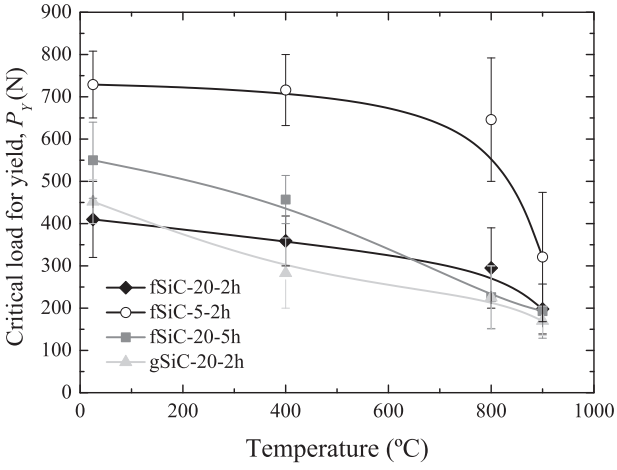

Fig. 7. Critical loads for the initiation of quasi-plastic damage, P_Y, in LPS-SiCs as a function of temperature. The data and error bars were determined as described in Section 2, and the solid lines are simple eye guides.

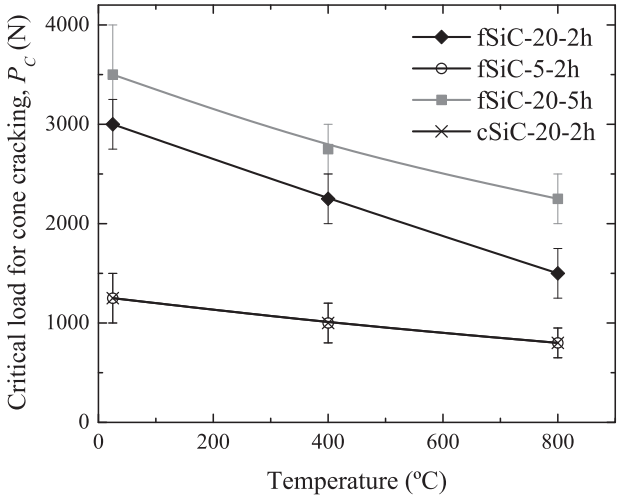

Fig. 8. Critical loads for the initiation of cone cracking, P_C, in LPS-SiCs as a function of temperature. The data and error bars were determined as described in Section 2, and the solid lines are included only as a guide to the eye.

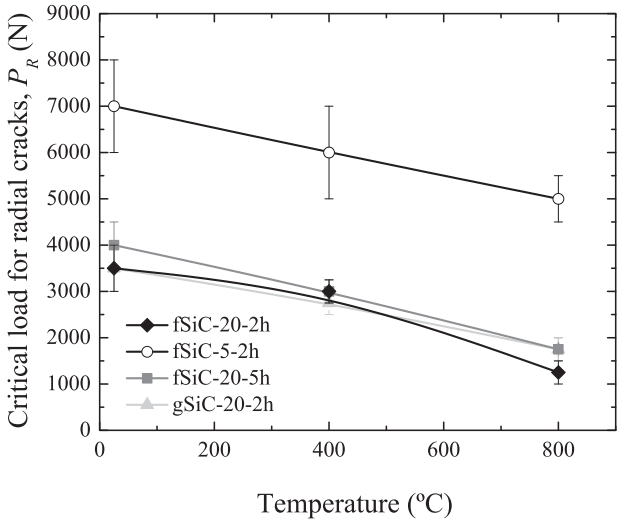

Fig. 9. Critical loads for the initiation of radial cracking, P_R, in LPS-SiCs as a function of temperature. The data and error bars were determined as described in Section 2, and the solid lines are included only as a guide to the eye.

5-2 h sample not only presents higher values over the whole temperature range, but also declines more slowly with increasing temperature, at least until approaching the creep temperature when a sharp drop is observed. The role of other microstructural features on the material's resistance to quasi-plastic damage is negligible compared to the amount of intergranular phase, and difficult to evaluate given the uncertainties in the data.

Quasi-plastic damage is the primary damage mode in all the LPS-SiC materials at all temperatures, since cone/ring cracking always occurs at higher critical loads as is shown in Fig. 8. This figure plots as a function of temperature the critical loads, P_C, for initiation of ring cracks on the material's surface, estimated as described in Section 2, with error bars indicating uncertainties and solid lines included only as a guide to the eye. All cracks observed were shallow, usually incomplete, ring cracks such as are shown in Fig. 6. Data for 900 °C has been excluded due to difficulties in determining the onset of cracking as a consequence of the initiation of oxidative processes on the material's surface at this temperature. Surface oxidation does not, however, prevent accurate measurement of the contact area since a clear contrast between the contact area and the surrounding surface is still obtained. The "ductility" of LPS-SiC ceramics (i.e., the fact that $P_C > P_Y$) is attributable to the heterogeneous microstructure developed in the presence of the intergranular phase and its ability to increase the material's toughness,[18,39] which also explains why ring cracks are unable to develop into full cone cracks. Fig. 8 demonstrates that the toughening ability seems to be little affected by the amount of intergranular phase—note that the fSiC-5-2 h and cSiC-20-2 h materials exhibit similar P_C values over the whole temperature range—and is favoured by elongated microstructures—fSiC-20-2 h, and especially fSiC-20-5 h, exhibit significantly larger P_C values, in good agreement with their measured room temperature toughness values (cf. Fig. 2). Again, grain size is shown to be important in increasing crack-bridging toughening[37] in the elongated microstructures, which explains why the P_C values for the fSiC-20-5 h sample are greater than for fSiC-20-2 h, but less so in the case of the less elongated microstructures, since the cSiC-20-2 h sample exhibits the same fracture resistance as the fSiC-5-2 h material.

Finally, Fig. 9 shows the critical loads for the initiation of radial cracks, P_R, as a function of temperature—just up to 800 °C as in the case of P_C, and for the same reasons—with error bars estimated as described in Section 2 and Bspline solid curves as a guide to the eye. Radial cracks appear in monolithic ceramics under contact stresses due to coalescence of microcracks associated with quasi-plastic damage,[40] and thus these monotonically decreasing curves resemble those of Fig. 7. The dominant role of the intergranular phase and the negligible effect of other microstructural features in quasi-plastic behaviour appears to be even clearer here. Indeed, an increment of 15 wt% in the amount of intergranular phase in most cases more than halves the critical load for the initiation of this extremely deleterious damage mode. In contrast, not even the increased toughness of elongated microstructures seems to significantly affect the onset of this damage mode in the samples with a higher amount of intergranular phase.

Therefore, in general, damage modes in LPS-SiCs at intermediate temperatures appear in the following order: quasi-plastic damage, cone cracking, and radial cracking, with the exception of the materials with elongated microstructures at 800 °C. At this temperature the increased toughness of these materials together with the faster decline of the yield stress with temperature produces radial cracking even before the first ring crack appears in the material's surface.

3. Conclusions and implications

The HTHT technique has been used to analyze the elasto-plastic behaviour and evolution of contact damage from room temperature up to 900 °C in various LPS-SiCs with distinct microstructural features. The results lead to the conclusion that the elasto-plastic properties of LPS-SiC at intermediate temperatures are degraded by increasing the amount of intergranular

phase. Especially worrisome has to be the reduction in the critical loads for radial crack initiation, since this damage mode seriously jeopardizes the mechanical integrity of the material. Moreover, the presence of the intergranular phase, even in small amounts, clearly reduces the material's creep resistance: all the LPS-SiCs studied showed evidence of creep under contact stresses at a relatively low temperature (compared to other ceramics[24–26]) of 1000 °C, and a clear degradation of their elasto-plastic properties even at 900 °C. The only somewhat beneficial effect of the presence of this intergranular phase is to allow the development of elongated, heterogeneous microstructures that enhance the toughness of the material.

Certainly, the other microstructural parameters studied (grain size and morphology) have a significant influence only on the toughness of the LPS-SiC materials at intermediate temperatures. Indeed, the crack-bridging toughening mechanism is enhanced by elongated grains, the more so the larger their size. This translates into a significant increase in the critical loads for ring cracking, which appears only as a secondary damage mode—at critical loads significantly larger than those for quasi-plastic damage and in some cases for radial cracking—and precludes their development into full cone cracks.

Therefore, the following fabrication guidelines can be suggested as inferred from the results of this study. In order to optimize the elasto-plastic properties of LPS-SiCs at intermediate temperatures, the amount of sintering additives should be minimal. Moreover, the additives should be selected so as to minimize the thermal expansion coefficient mismatch between the SiC grains and the resulting intergranular phase. This will increase the strength of the grain boundaries, delaying the onset of quasi-plastic damage (i.e., yield) and the temperature at which the elastic modulus degrades by reversible grain boundary sliding. Conversely, if toughness is the main concern, elongated microstructures with weak interfaces should be sought. Elongated microstructures can be achieved by facilitating SiC phase transformations through the selection of submicrometre starting powders rich in stacking-faults, a sufficient amount of sintering additives, an argon sintering atmosphere, and long sintering times.[28,34,41]

Acknowledgements

The authors wish to thank Dr A.L. Ortiz for his guidance in the analysis of the XRD data and many useful discussions.

This work was funded by the Ministerio de Ciencia e Innovación (PET2008_0168_02 and MAT2007-61609), the Consejería de Economía, Comercio e Innovación de la Junta de Extremadura (GRU09083), and FEDER funds.

References

1. Padture NP. In situ-toughened silicon-carbide. *J Am Ceram Soc* 1994;**77**:519–23.
2. Mulla MA, Krstic VD. Mechanical-properties of beta-SiC pressureless sintered with Al_2O_3 additions. *Acta Metall Mater* 1994;**42**:303–8.
3. Rodriguez-Rojas F, Borrero-Lopez O, Ortiz AL, Guiberteau F. Oxidation behavior of pressureless liquid-phase-sintered alpha-SiC in ambient air at elevated temperatures. *J Mater Res* 2008;**23**:1689–700.
4. Jensen RP, Luecke WE, Padture NP, Wiederhorn SM. High-temperature properties of liquid-phase-sintered alpha-SiC. *Mater Sci Eng A: Struct Mater Prop Microstruct Process* 2000;**282**:109–14.
5. Borrero-Lopez O, Ortiz AL, Guiberteau F, Padture NP. Microstructural design of sliding-wear-resistant liquid-phase-sintered SiC: an overview. *J Eur Ceram Soc* 2007;**27**:3351–7.
6. Xu HHK, Padture NP, Jahanmir S. Effect of microstructure on material-removal mechanisms and damage tolerance in abrasive machining of silicon-carbide. *J Am Ceram Soc* 1995;**78**:2443–8.
7. Sigl LS. Thermal conductivity of liquid phase sintered silicon carbide. *J Eur Ceram Soc* 2003;**23**:1115–22.
8. Biswas K, Rixecker G, Aldinger F. Improved high temperature properties of SiC-ceramics sintered with Lu_2O_3-containing additives. *J Eur Ceram Soc* 2003;**23**:1099–104.
9. Shimoda K, Eiza N, Park JS, Hinoki T, Kohyama A, Kondo S. High-temperature mechanical property improvements of SiC ceramics by NITE process. *Mater Trans* 2006;**47**:1204–8.
10. Kim YW, Mitomo M, Nishimura T. High-temperature strength of liquid-phase-sintered SiC with Aln and Re_2O_3 (Re = Y, Yb). *J Am Ceram Soc* 2002;**85**:1007–9.
11. Dapkunas SJ. Ceramic heat-exchangers. *Am Ceram Soc Bull* 1988;**67**:388–91.
12. Richerson DW. *Modern ceramic engineering. Properties, processing and use in design*. Boca Raton, FL: CRC Press; 2006.
13. Borrero-Lopez O, Ortiz AL, Guiberteau F, Padture NP. Effect of liquid-phase content on the contact-mechanical properties of liquid-phase-sintered alpha-SiC. *J Eur Ceram Soc* 2007;**27**:2521–7.
14. Borrero-Lopez O, Pajares A, Ortiz AL, Guiberteau F. Hardness degradation in liquid-phase-sintered SiC with prolonged sintering. *J Eur Ceram Soc* 2007;**27**:3359–64.
15. Borrero-Lopez O, Ortiz AL, Guiberteau F, Padture NP. Room-temperature mechanical properties of liquid-phase-sintered alpha-SiC with Y_2O_3–Al_2O_3 additions. *Bol Soc Esp Ceram V* 2005;**44**:265–9.
16. Ortiz AL, Munoz-Bernabe A, Borrero-Lopez O, Dominguez-Rodriguez A, Guiberteau F, Padture NP. Effect of sintering atmosphere on the mechanical properties of liquid-phase-sintered SiC. *J Eur Ceram Soc* 2004;**24**:3245–9.
17. Padture NP, Lawn BR. Contact fatigue of a silicon-carbide with a heterogeneous grain-structure. *J Am Ceram Soc* 1995;**78**:1431–8.
18. Padture NP, Lawn BR. Toughness properties of a silicon-carbide with an in-situ induced heterogeneous grain-structure. *J Am Ceram Soc* 1994;**77**:2518–22.
19. Xu KHK, Wei LH, Padture NP, Lawn BR, Yeckley RL. Effect of microstructural coarsening on hertzian contact damage in silicon-nitride. *J Mater Sci* 1995;**30**:869–78.
20. Melendez-Martinez JJ, Castillo-Rodriguez M, Dominguez-Rodriguez A, Ortiz AL, Guiberteau F. Creep and microstructural evolution at high temperature of liquid-phase-sintered silicon carbide. *J Am Ceram Soc* 2007;**90**:163–9.
21. Gallardo-Lopez A, Munoz A, Martinez-Fernandez J, Dominguez-Rodriguez A. High-temperature compressive creep of liquid phase sintered silicon carbide. *Acta Mater* 1999;**47**:2185–95.
22. Roebben G, Duan RG, Sciti D, Van Der Biest O. Assessment of the high temperature elastic and damping properties of silicon nitrides and carbides with the impulse excitation technique. *J Eur Ceram Soc* 2002;**22**:2501–9.
23. Sanchez-Gonzalez E, Melendez-Martinez JJ, Pajares A, Miranda P, Guiberteau F, Lawn BR. Application of Hertzian tests to measure stress–strain characteristics of ceramics at elevated temperatures. *J Am Ceram Soc* 2007;**90**:149–53.
24. Sanchez-Gonzalez E, Miranda P, Melendez-Martinez JJ, Guiberteau F, Pajares A. Contact properties of yttria partially stabilized zirconia up to 1000 degrees C. *J Am Ceram Soc* 2007;**90**:3572–7.
25. Sanchez-Gonzalez E, Miranda P, Melendez-Martinez JJ, Guiberteau F, Pajares A. Temperature dependence of mechanical properties of alumina up to the onset of creep. *J Eur Ceram Soc* 2007;**27**:3345–9.
26. Sanchez-Gonzalez E, Miranda P, Guiberteau F, Pajares A. Effect of temperature on the pre-creep mechanical properties of silicon nitride. *J Eur Ceram Soc* 2009;**29**:2635–41.

27. Zamora V, Sanchez-Gonzalez E, Ortiz AL, Miranda P, Guiberteau F. Hertzian indentation of a ZrB_2–30% SiC ultra-high-temperature ceramic up to 800 °C in air. *J Am Ceram Soc* 2010;**93**: 1848–51.
28. Xu HW, Bhatia T, Deshpande SA, Padture NP, Ortiz AL, Cumbrera FL. Microstructural evolution in liquid-phase-sintered SiC. Part I. Effect of starting powder. *J Am Ceram Soc* 2001;**84**:1578–84.
29. Ortiz AL, Cumbrera FL, Sanchez-Bajo F, Guiberteau F, Xu HW, Padture NP. Quantitative phase-composition analysis of liquid-phase-sintered silicon carbide using the Rietveld method. *J Am Ceram Soc* 2000;**83**: 2282–6.
30. Anstis GR, Chantikul P, Lawn BR, Marshall DB. A critical-evaluation of indentation techniques for measuring fracture-toughness. 1. Direct crack measurements. *J Am Ceram Soc* 1981;**64**:533–8.
31. Tabor D. *The hardness of metals*. London, U.K.: Oxford University Press; 1951.
32. Lawn BR. Indentation of ceramics with spheres: a century after Hertz. *J Am Ceram Soc* 1998;**81**:1977–94.
33. Johnson KL. *Contact mechanics*. Cambridge, U.K.: Cambridge University Press; 1985.
34. Deshpande SA, Bhatia T, Xu HW, Padture NP, Ortiz AL, Cumbrera FL. Microstructural evolution in liquid-phase-sintered SiC. Part II. Effects of planar defects and seeds in the starting powder. *J Am Ceram Soc* 2001;**84**:1585–90.
35. Dewith G, Parren RT. Translucent $Y_3Al_5O_{12}$ ceramics – mechanical-properties. *Solid State Ionics* 1985;**16**:87–93.
36. Xu HL, Jiang ZK. Dynamics of visible-to-ultraviolet upconversion in $YAlO_3$:1% Er^{3+}. *Chem Phys* 2003;**287**:155–9.
37. Lawn BR. *Fracture of brittle solids*. Cambridge, U.K.: Cambridge University Press; 1993.
38. Borrero-Lopez O, Ortiz AL, Guiberteau F, Padture NP. Effect of microstructure on sliding-wear properties of liquid-phase-sintered alpha-SiC. *J Am Ceram Soc* 2005;**88**:2159–63.
39. Pajares A, Wei LH, Lawn BR, Padture NP, Berndt CC. Mechanical characterization of plasma sprayed ceramic coatings on metal substrates by contact testing. *Mater Sci Eng A: Struct Mater Prop Microstruct Process* 1996;**208**:158–65.
40. Cai HD, Kalceff MAS, Lawn BR. Deformation and fracture of mica-containing glass–ceramics in Hertzian contacts. *J Mater Res* 1994;**9**:762–70.
41. Ortiz AL, Bhatia T, Padture NP, Pezzotti G. Microstructural evolution in liquid-phase-sintered SiC. Part III. Effect of nitrogen-gas sintering atmosphere. *J Am Ceram Soc* 2002;**85**:1835–40.